A STUDY OF LARGE-SCALE STRUCTURE IN TURBULENT EKMAN LAYER THROUGH DNS

Kenji Shingai, Hiroshi Kawamura
Department of Mechanical Engineering,
Tokyo University of Science
Yamasaki 2641, Noda-shi, Chiba 278-8510, Japan
a7501701@rs.noda.tus.ac.jp, kawa@rs.noda.tus.ac.jp

ABSTRACT

The direct numerical simulations (DNSs) of the turbulent Ekman layer over a smooth flat surface are performed. The Reynolds numbers are set to be $Re_f = 400$, 510 and 600 where Re_f is defined by $Re_f = G/\sqrt{((\nu f)/2)}$ with use of the geostrophic wind velocity G, kinematic viscosity ν and Coriolis parameter f. The result with a higher Reynolds number of 600 shows a logarithmic region. However the slope is different from that of the turbulent Poiseuille flow because of its three-dimensional nature. The characteristics of the streak structure in the vicinity of the wall and large-scale structure in far upper region are discussed based on the obtained statistics such as pre-multiplied energy spectra. The effect of Reynolds number onto the large-scale structure is also discussed.

INTRODUCTION

The planetary boundary layer (PBL) is affected by the system rotation. The boundary layer under the effect of the rotation is called as the Ekman layer. The calculation of the turbulent Ekman layer provides fundamental and important information about the three-dimensional turbulent boundary layer and PBL.

It is well known that horizontal roll vortices are caused by buoyancy or inflectional instability in the laminar Ekman layer. Coleman et al.(1990) performed the direct numerical simulation (DNS) of the turbulent Ekman layer with a low Reynolds number, and found that no horizontal roll vortices appeared under the neutral stratification.

Existence of large-scale structures in the wall turbulence with a high Reynolds number is reported recently. Several DNSs of turbulence with simple boundary condition such as the turbulent channel flow are being made in order to obtain detail information about the large-scale structures.

In the present work, the neutrally stratified turbulent Ekman layer with higher Reynolds numbers of $Re_f = 510$ and 600 are computed through the DNS, where Re_f is defined by

$$Re_f = \frac{G}{\sqrt{(\nu f)/2}} \tag{1}$$

with use of the geostrophic wind velocity G, kinematic viscosity ν and Coriolis parameter f. The effects of the Reynolds number upon the statistical quantities are examined based on the obtained DNS data. Moreover, the characteristics of the turbulent structure appearing in the vicinity of the wall and large-scale structure in the high-upper region will be also discussed.

NUMERICAL PROCEDURES

Calculated flow field is the turbulent Ekman layer of an incompressible viscous fluid over a smooth flat surface. The system is rotating about a vertical axis with an angler velocity $\boldsymbol{\Omega} = (0, f, 0)$.

The flow is driven by the combination of the horizontal pressure gradient and the Coriolis force. The computational configuration is given in figure 1. Periodic boundary conditions are imposed in the x and z directions. The non-slip and the Neumann conditions are adopted at the bottom and top boundaries.

The governing equations are the continuity

$$\nabla \cdot \boldsymbol{u} = 0, \tag{2}$$

and the Navier-Stokes equations

$$\frac{\partial \boldsymbol{u}}{\partial t} + (\boldsymbol{u} \cdot \nabla)\,\boldsymbol{u} + 2\boldsymbol{\Omega} \times \boldsymbol{u} = -\frac{1}{\rho}\nabla p + \nu \nabla^2 \boldsymbol{u}, \tag{3}$$

where t, $\boldsymbol{u}$, p and ρ are the time, the velocity vector, the pressure and the density of fluid, respectively.

In the present computation, the fractional step method is adopted for the coupling between the continuity and the Navier-Stokes equations. The 2nd-order Crank-Nicolson and the 2nd-order Adams-Bashforth methods are employed as the time-advance algorithm; the former for the vertical viscous term, the latter for the other viscous and the convection terms. The Coriolis term is solved implicitly to avoid the numerical instability. The finite difference method is used for the spatial discretization. A 4th-order central difference scheme proposed by Morinishi (1995) is adopted in the

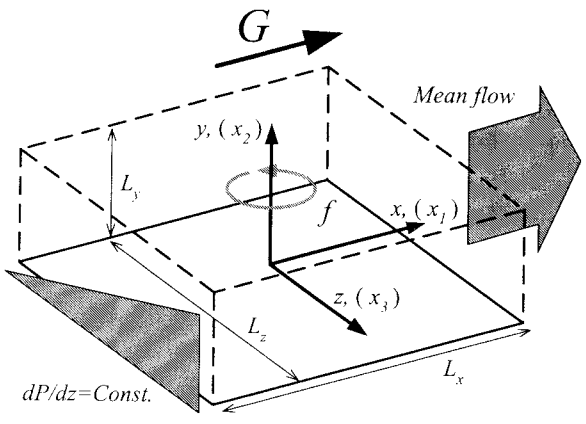

Figure 1: Configuration.

Table 1: Computational conditions.

	Coleman et al.(1990)	present		
Re_f	400	400	510	600
Re	-	8000	13000	18000
Ro	-	10.0	10.0	10.0
L_x, L_y, L_z	$2.0\delta_\tau, \infty, 2.0\delta_\tau$	$4.61\delta_\tau, 1.54\delta_\tau, 4.61\delta_\tau$	$6.52\delta_\tau, 1.63\delta_\tau, 6.52\delta_\tau$	$5.08\delta_\tau, 1.69\delta_\tau, 5.08\delta_\tau$
L_x^+, L_y^+, L_z^+	$672, \infty, 672$	$1,560, 521, 1,560$	$3,190, 798, 3,190$	$3,190, 1,060, 3,190$
N_x, N_y, N_z	$96, 45, 96$	$256, 96, 256$	$512, 160, 512$	$512, 160, 512$
$\Delta x^+, \Delta z^+$	$7.0, 7.0$	$6.11, 6.11$	$6.23, 6.23$	$6.23, 6.23$
Δy^+	$0.2 -$	$0.148 - 14.5$	$0.177 - 12.5$	$0.150 - 18.5$

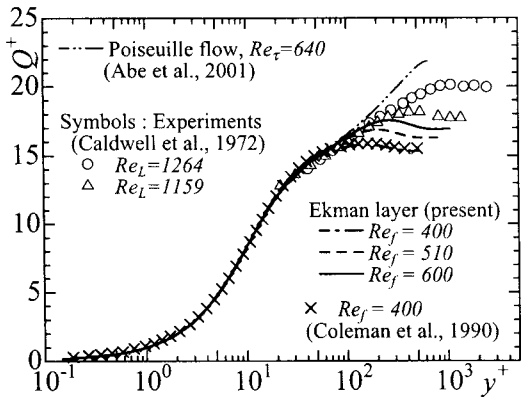

Figure 2: Mean velocity profiles.

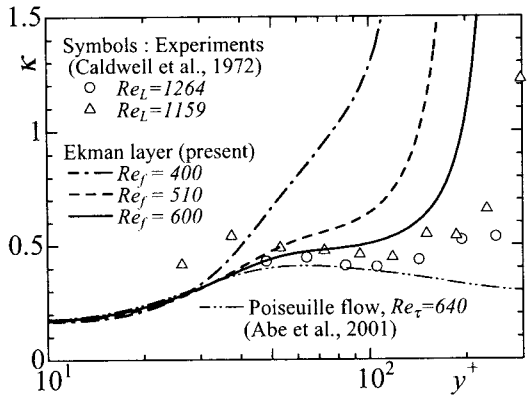

Figure 3: Near wall distributions of von Kármán constants.

streamwise (x) and spanwise (z) directions, and the 2nd-order central difference scheme is used in the wall-normal (y) direction.

The non-dimensional parameters used in the present calculation are the Reynolds Re and Rossby numbers Ro. They are defined by

$$Re = \frac{Gh}{\nu}, Ro = \frac{G}{fh}, \tag{4}$$

where h is the height of the computational domain. The computational conditions are summarized in table 1, where L_x, L_y and L_z are the lengths of computational domain and N_x, N_y and N_z are the number of grid points in x, y and z directions, respectively. The lengths of computational domain are described with use of the turbulent depth $\delta_\tau = u_\tau/f$, where u_τ is the friction velocity. The superscript $^+$ indicates that the variables are normalized by ν and u_τ. The discretizations in each direction are given by Δx^+, Δy^+ and Δz^+. The height of computational domain is so set to be enough large compared to the boundary layer thickness. The much larger horizontal domain is adapted compared with that of Coleman et al.(1990).

RESULTS AND DISCUSSION

Mean Velocity Profiles

The absolute values of mean velocity Q^+ as a function of height y^+ are given in figure 2 and compared with the experiments of Caldwell et al.(1972). The Reynolds number Re_L is defined by $Re_L = G/\sqrt{\Omega_L \nu}$, where Ω_L is the angular velocity of the plate rotation. The DNS of the turbulent Ekman layer by Coleman et al.(1990) and the one of the turbulent Poiseuille flow by Abe et al.(2001) are also shown for comparison.

The profile for $Re_f = 400$ shows good agreement with that of Coleman et al.(1990). Both of these results indecate that the logarithmic region is not obtained in the case of $Re_f = 400$. On the other hands, in the case of the highest Reynolds number $Re_f = 600$, the logarithmic region is observed. Present result with $Re_f = 600$ shows good agreement with the experiments by Caldwell et al.(1972) in the logarithmic region. The comparison with the turbulent Poiseuille flow points out that the slope of logarithmic region in the turbulent Ekman layer is smaller than that of the Poiseuille flow. The logarithmic region for the mean velocity distribution is expressed as

$$Q^+ = \frac{1}{\kappa} \ln y^+ + B, \tag{5}$$

where κ and B are the von Kármán and the additive constants. Figure 3 shows the distributions of von Kármán constants. In the case of $Re_f = 600$, κ stays at a roughly constant value of $0.45 - 0.5$ in the region of $y^+ = 50 - 100$. The values obtained in experiments by Caldwell et al.(1972) agree well with the present result. This indicates that the von Kármán constants in the turbulent Ekman layer increase if compared with the well-known $\kappa \sim 0.4$ in the non-rotating wall turbulence. In fact, figure 3 indicates that κ in turbulent Ekman layer is higher than that of the turbulent Poiseuille flow calculated by Abe et al.(2001). This is due to the three-dimensional nature of the turbulent Ekman layer. Moin & Shih (1990) and Pierce & McAllister (1983) investigated the three-dimensional turbulence through numerical and experimental procedures, respectively. They also reported the increase of κ in the three-dimensional turbulence.

The hodographs of the mean velocities for $Re_f = 400$, 510 and 600 are given in figure 4. The analytical solution in the laminar Ekman layer is also shown. The spiral shrinks as the increase of Reynolds number. This means that the

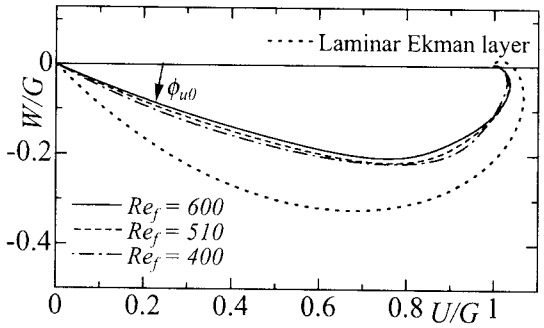

Figure 4: Hodographs of mean velocities.

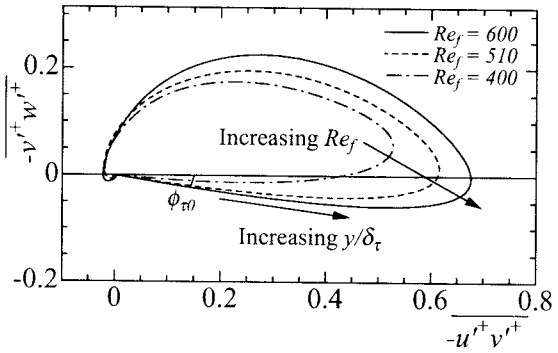

Figure 5: Hodographs of projected Reynolds stress tensor onto horizontal plane.

mean flow direction becomes closer to that of the geostrophic wind. The angles ϕ_{u0} between the shear direction at wall and the geostrophic wind direction are shown in table 2. The analytical solution of the laminar Ekman layer gives 45 degrees. However, the angles ϕ_{u0} in the turbulent Ekman layer decrease to smaller values of $23-28$ degrees. Caldwell et al.(1972) also obtained smaller angles of $\phi_{u0} = 19-28$ in his experiments. As for the Reynolds number dependence, the angle ϕ_{u0} decreases as the increase of Reynolds number. This is because the momentum transfer to the vertical direction is enhanced in the case of higher Reynolds number. Therefore the momentum of geostrophic wind for the higher Reynolds number penetrates more deeply into the near wall region. Caldwell et al.(1972) did not found any definite dependence of ϕ_{u0} upon Re, probably because of the difficulty in the measurement. On the other hands, in the stably stratified Ekman layer, Shingai & Kawamura (2002) found the weakened momentum transfer caused the increase of the angle ϕ_{u0}.

Reynolds Shear Stress

In order to examine the three-dimensional characteristics of Reynolds shear stress, the hodographs of the projected Reynolds shear stress tensors onto the horizontal plane $\left(-\overline{u'v'}, -\overline{v'w'}\right)$ are shown in figure 5. These hodographs show an oval-shaped profile. They expand as the Reynolds

Table 2: Mean shear direction at the ground.

	Laminar	Turbulence		
Re_f	-	400	510	600
ϕ_{u0} [Deg.]	45.0	28.3	25.4	23.3

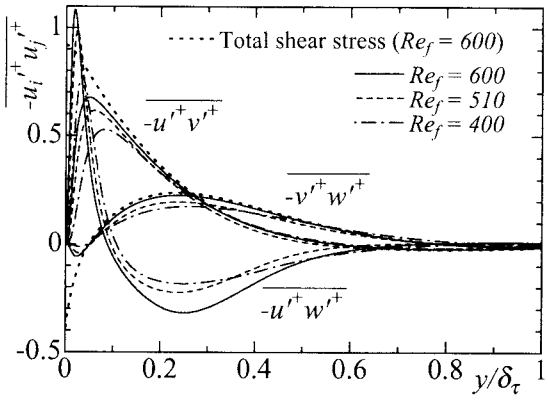

Figure 6: Reynolds stress components as functions of height.

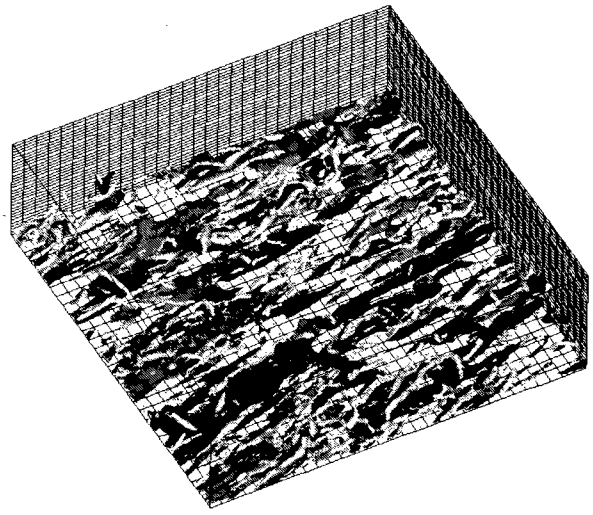

Figure 7: Instantaneous velocity field for $Re_f = 600$. Gray : high-speed region $u_s'^+ > 2.8$, dark gray : low-speed region $u_s'^+ < -2.8$, white : second invariant of velocity gradient tensor $II^+ < -0.028$.

number increases because the velocity fluctuations are enhanced. The expansion or the shrinkage of the hodographs of the projected Reynolds shear stress tensors were also observed in the stratified Ekman layer (Shingai & Kawamura, 2002). One may notice, however, a significant difference in the way to expand or shrink of the hodograph of the projected Reynolds shear stresses. That is, the hodograph expands with its shape unchanged in the case of stratified Ekman layer, while those obtained in the present calculation extend especially into the fourth quadrant with the increases of Reynolds number. This is because the components of Reynolds shear stresses in the vicinity of the wall are very sensitive to the variation of the Reynolds number. Figure 6 shows the profiles of the Reynolds stress components as the functions of the height. The components $-\overline{u'v'}$ and $-\overline{v'w'}$ increase in the vicinity of the wall with the increase of the Reynolds number, while they are almost constant in the re-

Table 3: Horizontal projected Reynolds stress direction near the ground.

Re_f	400	510	600
$\phi_{\tau 0}$ [Deg.]	4.73	7.75	8.86

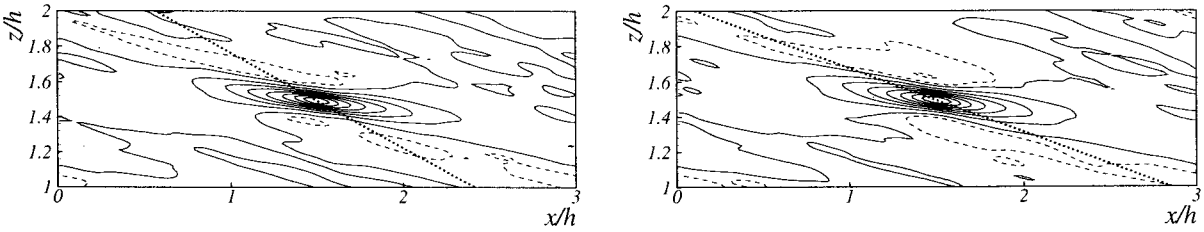

(a) $y^+ = 0.148$ (b) $y^+ = 10.0$

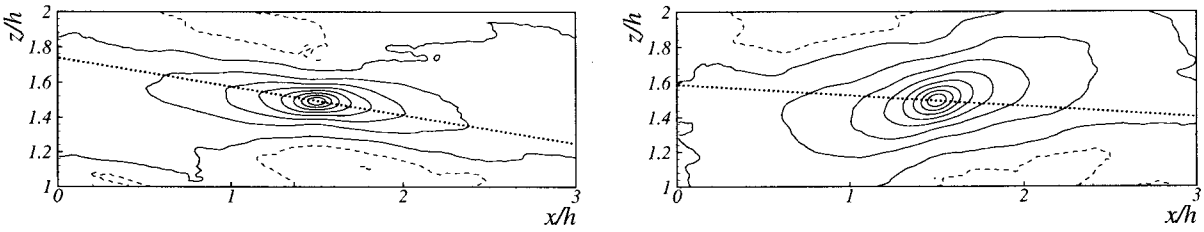

(c) $y^+ = 52.8$ (d) $y^+ = 119$

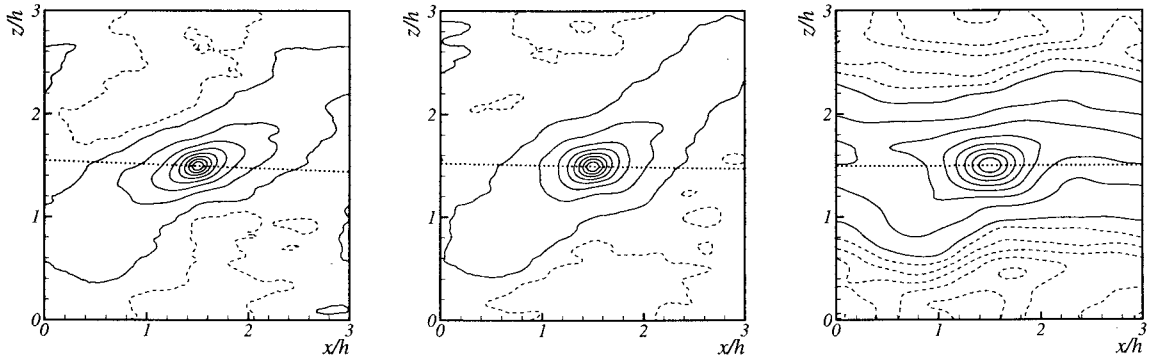

(e) $y^+ = 152$ (f) $y^+ = 193$ (g) $y^+ = 427$

Figure 8: Contours of two dimensional two-point correlations of streamwise velocity fluctuations in horizontal planes for $Re_f = 400$. Solid lines, $R_{uu} \geq 0$ contour interval 0.125 ; dashed lines, $R_{uu} < 0$ contour interval 0.0625 ; dotted straight lines, mean velocity directions.

gion of $y/\delta_\tau > 0.4$. As the results, the part of the hodograph described by the vectors in the vicinity of the wall expands more significantly than the other parts.

The angles $\phi_{\tau 0}$ between the vectors $(-\overline{u'v'}, -\overline{v'w'})$ in the vicinity of the wall and the geostrophic wind vector G are compared in the table 3. The angle $\phi_{\tau 0}$ increases with the increase of the Reynolds number. This is not in accordance with the mean shear direction at the wall ϕ_{u0} shown in table 2. This is because the Reynolds shear stress components increase with the growth of the Reynolds number especially in the vicinity of the wall as described above. The peak points of $-\overline{u'v'}$ and $-\overline{v'w'}$ move towards the wall and the values approach to the total shear stress with the increase of Reynolds number. Therefore, the both angles ϕ_{u0} and $\phi_{\tau 0}$ tend to converge.

Turbulent Structures in the Vicinity of the Wall

The instantaneous flow field for $Re_f = 600$ are illustrated in figure 7. The isosurfaces colored by gray and dark gray show the high- and low-speed regions, respectively. Here, the velocity fluctuation u'_s means the fluctuation parallel to the mean velocity direction at each height. The white one shows the second invariant of the velocity gradient tensors $II^+ < -0.028$, corresponding to the central regions of the vortices. The well-known streak structures are observed in the vicinity of the wall.

In order to investigate the three-dimensional characteristics of the turbulent structures, the two-point correlations of streamwise velocity fluctuations on the horizontal plane at each height are displayed in figure 8, where contour interval is 0.125 and the dashed lines correspond the negative correlations. The dotted straight lines show the mean flow direction at each height. The high contour levels would be much more elongated in the direction parallel to the structure. In the near wall region ($y^+ \leq 52.8$), many of the structures are

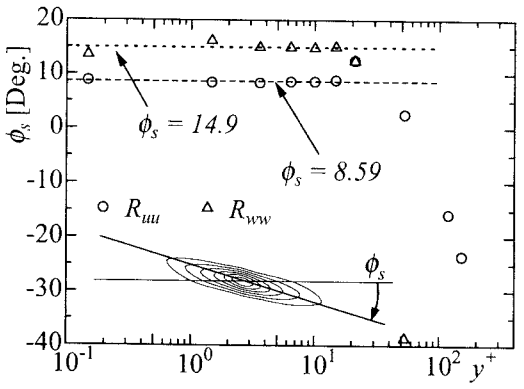

Figure 9: Structure directions estimated by two-dimensional two-point correlations R_{uu} and R_{ww} in the vicinity of the wall.

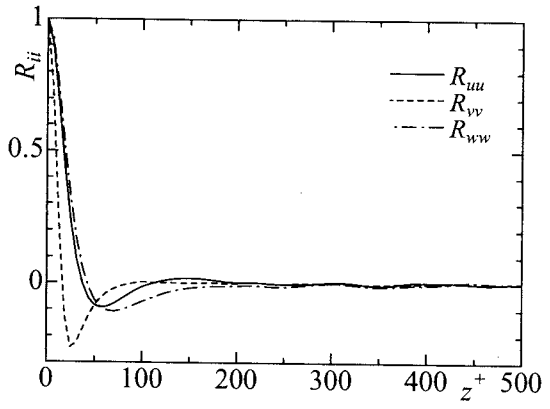

Figure 10: Spanwise two-point correlation R_{ii} for $Re_f = 600$ at $y^+ = 5.05$.

elongated along the direction of the mean pressure gradient. However, the mean directions of the structures are not parallel to the mean flow directions. The mean directions in the vicinity of the wall are independent of the change of the height and almost constant. On the other hands, those of the upper region changes appreciably with the change of the height. The mean directions of the structures are plotted in figure 9 as the angle ϕ_s against the geostrophic wind direction. The both angles ϕ_s of R_{uu} and R_{ww} are constant in the region of $y^+ < 20$. However, in the upper region of $y^+ > 20$, they decrease with the increase of the height. Moreover, the angle of R_{uu} falls down to the opposite of the pressure gradient direction in the region of $y^+ > 100$.

The spacing of the streak structures are obtained from the near-wall negative peak of the spanwise two-point correlations R_{uu} and R_{ww}. The near-wall two-point correlations for $Re_f = 600$ are shown in figure 10. The negative peaks of R_{uu} and R_{ww} appear at $z^+ = 56.1$ and 68.5, respectively. Since the streaks are not perpendicular to the z direction, the real spacing between the streaks must be accomodated with the use of the inclination angle ϕ_s. After the accomodation, one obtains the spacing of the streak structures as $l_z^+ = 111 - 132$, which agrees well with $l_z^+ \sim 100$ known for the non-rotating wall turbulence such as the turbulent Poiseuille flow.

A close inspection of figure 7 indecates that many arch or horseshoe shaped vortices exist in turbulent Ekman layer.

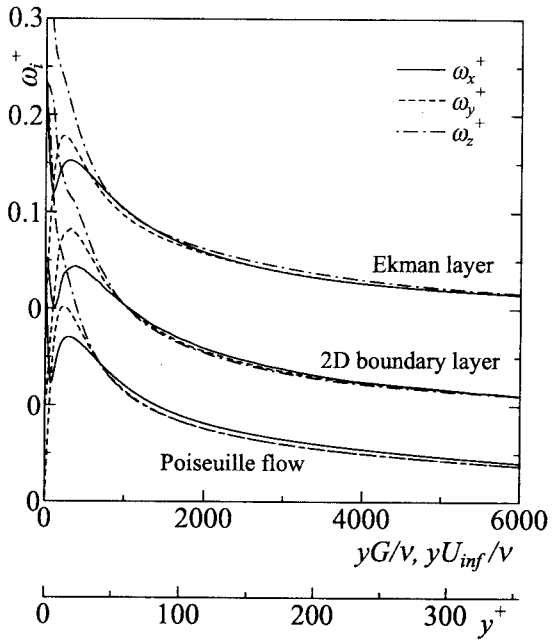

Figure 11: Vorticities distribution for Ekman layer ($Re_f = 600$), two-dimensional boundary layer (Spalart, 1986) and Poiseuille flow (Abe et al., 2001). (Note that the origin is shifted for each plot.)

Three components of the vorticities are shown in figure 11. Those in the turbulent Poiseuille flow calculated by Abe et al.(2001) and in the non-rotating turbulent boundary layer by Spalart (1986) are also plotted for comparison. The profiles in the Poiseuille flow are shown as a function of y^+ and those in turbulent boundary layer as a function of yU_{inf}/ν, where U_{inf} means the velocity in the far upper region.

Robinson (1991) proposed an idealized model for the turbulent boundary layers based on the vortical structures. In his model, arch or horseshoe shaped vortices dominate in the wake region ($y^+ > 100$). However, in the two-dimensional wall turbulence, the spanwise component of the vorticity ω_z stays at a lower value than the other components in the region of $y^+ > 100$. On the other hands, in the turbulent Ekman layer, ω_z becomes the highest component among the three. This is an evidence of the complicated vortical structures with many arch or horseshoe shaped vortices in the turbulent Ekman layer.

Large-Scale Structures

In order to examine the existence of the large-scale structures, the pre-multiplied energy spectra $k_z E_{uu}$ of $Re_f = 600$ is given in figure 12, referring to Jiménez (1998). Here, E_{uu} means the energy spectrum of the streamwise velocity and k_z is spanwise wave number. Since the pre-multiplied spectrum is proportional to the power in a logarithmic band at k_z, its peak indicates the wavelength of the energy-containing scale. The wavelength λ_z containing the largest energy increases with the increase of the height.

The spanwise wavelengths λ_z containing the largest energy at each height for $Re_f = 400$, 510 and 600 are plotted in figure 13. This figure shows the profiles the length-scale of the most energetic structure as a function of the height. In the wall vicinity, the wavelength stays at a constant value of $\lambda^+ \sim 100$. This corresponds to the streak structures. In the middle region of $y/\delta_\tau < 0.4$, the length-scales for

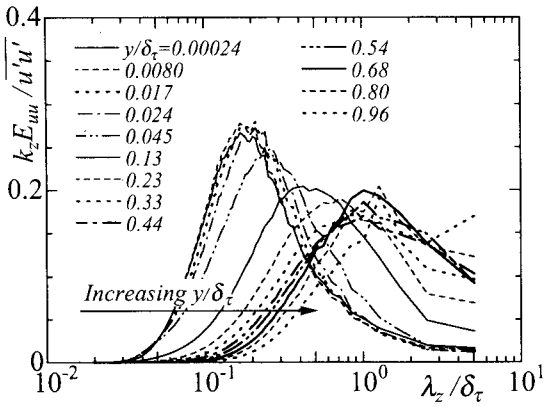

Figure 12: Pre-multiplied power spectra $k_z E_{uu}$ for $Re_f = 600$.

$Re_f = 510$ and 600 increase linearly with the growth of the height. In the non-rotating system, the similar linear increasing region is obtained by Jiménez (1998) and by Abe & Kawamura (2002). In the far upper region ($y/\delta_\tau > 0.4$), the wavelengths of the most energetic structures again keep a constant value of $\lambda/\delta_\tau \sim 1.0 - 1.3$. This means the existence of the large-scale structures with the spanwise spacing of $1.0\delta_\tau - 1.3\delta_\tau$. In the case of low-Reynolds number $Re_f = 400$, the profiles of λ_z differ from those of the other cases. This seems to be caused by the low-Reynolds number effect and the narrow computational domain.

In the case of the turbulent Poiseuille flow, $k_z E_{uu}$ in the central region shows a sharp peak at its maximum point. Moreover, $k_z E_{uu}$ in the near wall regions has secondary maxima corresponding to the length-scale of the large-scale structures (Abe & Kawamura, 2002). However, the profiles of $k_z E_{uu}$ in the Ekman layer shows a dull rounded profiles in the upper region and don't have the secondary maxima in the near wall region. This indicates that the turbulent Ekman layer is less affected by the large-scale structures than that of the Poiseuille flow. This is probably because the three-dimensional nature of the turbulent Ekman layer prevents the growth of the large structure.

CONCLUSIONS

The direct numerical simulations of turbulent Ekman layer over a smooth flat surface performed. The Reynolds number is set to be $Re_f = 400$, 510 and 600, where the Reynolds number Re_f is based on the geostrophic wind G and the Coriolis parameter f. The Reynolds number dependences of the low order turbulent statistics are examined. The characteristics of the turbulent structures are also discussed based on the obtained DNS data. The conclusions are derived as follows;

- The logarithmic region is obtained in the higher-Reynolds number case of $Re_f = 600$. The slope of the logarithmic region in the Ekman layer decreases compared with the two-dimensional wall turbulence.
- Not only the size but also the shape of the hodograph of the projected Reynolds stress tensor onto the horizontal plane varies with the increase of the Reynolds number.
- The well-known streak structures appear in the vicinity of the wall. On the other hands, the complicated vortex structures are obtained in the middle-height region.

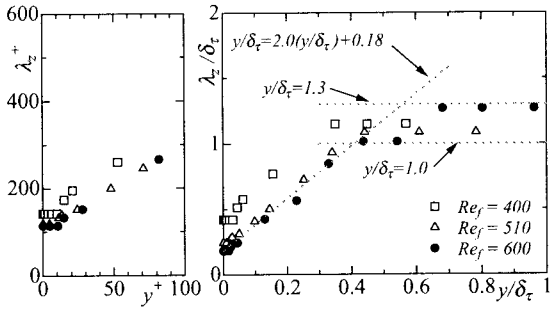

Figure 13: Spanwise wavelength of the maxima of the pre-ultiplied spectra for $Re_f = 400$, 510 and 600.

- The investigation using the pre-multiplied power spectra indicates that the large-scale structures with a spanwise wavelength of $1.0\delta_\tau - 1.3\delta_\tau$ exist in the far upper region.

The present simulations were performed with the use of VPP5000/3 of Tokyo University of Science and VPP5000/64 at the Computer Center of Nagoya University.

REFERENCES

Abe, H., Kawamura, H., and Matsuo, Y., 2001, "Direct numerical simulation of a fully developed turbulent channel flow with respect to the Reynolds number dependence", *Trans. ASME J. Fluids Eng.*, Vol. 123, pp. 382-393.

Abe, H., and Kawamura, H., 2002, "A study of turbulence thermal structure in a channel flow through DNS up to $Re_\tau = 640$ with $Pr = 0.025$ and 0.71", *Proceedings, 9th European Turbulence Conference*, I. P. Castro et al., ed., CIMNE, Barcelona, pp. 399-402.

Caldwell, D. R., Van Atta, C. W., and Helland, K. N., 1972, "A laboratory study of the turbulent Ekman layer", *Geophy. Fluid Dyn.*, Vol. 3, pp. 125-160.

Coleman, G. N., Ferziger, J. H., and Spalart, P. R., 1990, "A numerical study of the turbulent Ekman layer", *J. Fluid Mech.*, Vol. 213, pp. 313-348.

Jiménez, J., 1998, "The largest scales of turbulent wall flows", CTR Annu. Research Briefs 1998, pp. 137-154.

Moin, P., and Shih, T.-H., 1990, "Direct numerical simulation of a three-dimensional turbulent boundary layer", *Phys. Fluids A*, Vol. 2, No. 10, pp. 1846-1853.

Morinishi, Y., 1995, "Conservative properties of finite difference scheme for incompressible flow", CTR Annu. Research Briefs 1995, Stanford Univ./NASA Ames, pp. 121-132.

Pierce, F. J., and McAllister, J. E., 1983, "Near-wall similarity in a shear-driven three-dimensional turbulent boundary layer", *Trans. ASME J. Fluids Eng.*, Vol. 105, pp. 263-269.

Robinson, S. K., 1991, "Coherent motions in the turbulent boundary layer", *Annu. Rev. Fluid Mech.*, Vol. 23, pp. 601-639.

Shingai, K., and Kawamura, H., 2002, "DNS of turbulent heat transfer in Ekman layer with stable stratification", *Proceedings, 9th European Turbulence Conference*, I. P. Castro et al., ed., CIMNE, Barcelona, pp. 217-220.

Spalart, P. R., 1986, "Numerical study of sink-flow boundary layers", *J. Fluid Mech.*, Vol. 172, pp. 307-328.